Improvements in Raman Lidar Measurements Using New Interference Filter Technology

Dr. David N. Whiteman

NASA/GSFC, Greenbelt, MD 20771

david.n.whiteman@nasa.gov

Mr. John R. Potter

Barr Associates, Westford, MA 01886

jpotter@barrassociates.com

Ms. Rebecca Tola

Barr Associates, Westford, MA 01886

rtola@barrassociates.com

Dr. Igor Veselovskii

University of Maryland, Baltimore County, Baltimore, MD 21250

iveselov@agnes.gsfc.nasa.gov

Mr. Martin Cadirola

Ecotronics, LLC, Clarksburg, MD 20871

cadirola@ecotronics.com

Mr. Kurt Rush

NASA/GSFC, Greenbelt, MD 20771

kurt.d.rush@nasa.gov

Mr. Joseph Comer

Science Systems and Applications Inc, Lanham, MD 2070

comer@agnes.gsfc.nasa.gov

1 Abstract

Narrow-band interference filters with improved transmission in the ultra-violet have been developed under NASA-funded research and used in the Raman Airborne Spectroscopic Lidar (RASL) in ground-based, upward-looking tests. Measurements were made of atmospheric water vapor, cirrus cloud optical properties and carbon dioxide that improve upon any previously demonstrated using Raman lidar. Daytime boundary and mixed layer profiling of water vapor mixing ratio up to an altitude of approximately 4 km is performed with less than 5% random error using temporal and spatial resolution of 2-minutes and 60 – 210, respectively. Daytime cirrus cloud optical depth and extinction-to-backscatter ratio measurements are made using 1-minute average. Sufficient signal strength is demonstrated to permit the simultaneous profiling of carbon dioxide and water vapor mixing ratio into the free troposphere during the nighttime. A description of the filter technology developments is provided followed by examples of the improved Raman lidar measurements.

2 Introduction

Raman Lidar is now regarded as one of the leading technologies for atmospheric profiling of water vapor [Melfi et. al, 1989] [Whiteman et. al., 1992] [Turner et. al., 2000], cirrus clouds [Ansmann et. al., 1992a] [Reichardt et. al., 2002] [Whiteman et. al., 2001a] [Whiteman et. al., 2004] and other quantities including aerosols [Ansmann et. al., 1990] [Ferrare et. al., 2005] and temperature [Arshinov et. al., 2005] [Behrendt et. al., 2002] [Di Girolamo et. al, 2004]. Experimental measurements using Raman lidar have been made of carbon dioxide [Riebesell, 1990] [Ansmann et. al., 1992b] as well. Traditionally, most Raman lidar measurements based on laser sources in the near-UV (approximately 350 nm) were limited to the nighttime. In the 1990s, advances in Raman lidar technology (high-power UV lasers and narrow-band interference filters) and techniques (narrow field-of-view detection) resulted in systems operating in the near-UV that measure water vapor and aerosols throughout the diurnal cycle [Turner et. al., 2000].

Interference filtering was one of the crucial technologies that permitted this extension of Raman lidar water vapor measurements to the daytime. Prior to the research undertaken here, daytime measurements of water vapor mixing ratio were typically made using interference filters with widths of 0.25 - 0.3 nm and peak transmissions of 30-40% at a wavelength of ~407.5 nm. It was therefore clear that significant lidar system performance gains could be realized through improvement in peak transmission of the water vapor interference filter being used since the statistical

uncertainty in the water vapor measurement dominates the error budget of a Raman Lidar water vapor mixing ratio measurement. Other measurement techniques, both passive and active, could also benefit from higher transmission interference filters due to the widespread use of interference filter technology in optical detection systems. For these reasons, the National Aeronautics Space Administration's (NASA) Advanced Component Technology (ACT) program funded a joint research effort between Barr Associates and NASA/Goddard Space Flight Center to develop and test advanced narrow-band, UV interference filters with up to twice the peak transmission while maintaining all other specifications of the filter the same. This implied that the physical size and weight of the filters and their rejection of out-of-band light would not change fmr previous technology. Therefore, the goal of the research was to develop and validate interference filters that significantly improve the measurement capability of remote sensing systems including lidars but do not add to the weight, volume or power requirements of the system.

3 Interference Filter Technology Development

The objectives of this research were to develop a process for fabricating UV filters with significant improvement in throughput, then to build and demonstrate a series of UV filters possessing 100 to 250 picometer bandwidths and peak transmission of 60-80%. Temperature stability and long lifetime were desired indicating that refractory oxides would be the thin film materials of choice. Among the filters developed under this activity were ones to measure Raman scattering from water

vapor, nitrogen and carbon dioxide when excited by the frequency-tripled Nd:YAG laser (354.71 nm). The specifications of these 50 mm diameter filters are shown in Table 1.

Various materials that have previously been found useful for fabrication of UV interference filters [Schink et. al., 1995] [MacLeod et. al, 1989], including tantalum pentoxide (Ta_2O_5), hafnium oxide (HfO_2) and zirconium oxide (ZrO_2), were studied as a part of this effort. Depositions were made using each of these materials in combination with silicon dioxide and then spectral comparisons were made. Three deposition processes were explored in order to make thin films using these materials. The focus was on optimizing these processes for minimal absorption, scattering and reflection losses on Fabry-Perot narrowband interference coatings. Electron beam, Kaufman ion-assisted deposition (IAD) [Pawlewicz, 1998], DC magnetron sputtering and ion beam sputtering (IBS) processes were compared as methods to deposit thin films for this research effort. Of the three processes investigated, the Kaufman IAD process yielded results closest to the design goals. Scattering losses on both the ion beam and magnetron sputter processes proved to be too great to achieve high throughput on ultra-narrowband UV filters. It was shown by initial experimentation that Zirconium dioxide (ZrO_2) had excessive scattering losses, as compared with Ta_2O_5. The major effort was, therefore, expended in optimizing filters constructed by layering Ta_2O_5 using the IAD process. This task was broken down into four separate elements; improving spatial uniformity, minimizing scatter losses, minimizing reflection losses and minimizing absorption losses. Each of these elements will now be addressed.

1. Wavelength and bandshape spatial uniformity were addressed with the goal of achieving less than 0.005% change in either parameter across a 50 mm diameter substrate. The experimentation led to three conclusions: a consistent substrate temperature is required during the deposition process, a substrate significantly larger than the final size of the part greatly improves the heat distribution and large clearances in front of and behind the substrate minimized the thermal effects on optical thickness distribution. Even at the end of this activity, however, consistent fabrication of spatially uniform 0.1 nm wide filters remained a challenge. Therefore, further work in process control is necessary to improve the yield of filters possessing spatially uniform wavelength and bandshape.

2. Minimizing scatter is critical to achieving maximum filter throughput. This is particularly important with very narrow bandwidth filters operating in the ultraviolet region because scattering sites are large compared with the filter center wavelength. Coatings were studied with a scatterometer demonstrating a correlation between increased scattering and transmission loss. As the bandwidth decreased, the transmittance decreased exponentially as a function of scattering. Experiments were performed during the manufacture of a 0.1 nm wide filter. The surface flatness that was required for maximum transmittance was ~0.10 nm (r.m.s.), as shown in Table 2. If films grew into a crystalline structure, the scattering would increase, therefore it was mandatory that the films be amorphous. Substrate temperature, ion beam flux, deposition rates and choice of materials all played a role in minimizing scatter. Minimizing contamina-

tion reduces scattering, so extra precautions were taken to ensure the substrate surface and the deposition system did not introduce additional scattering due to contaminants.

3. Minimizing reflection losses starts with a thin film design where each filter component is matched to its media such that the reflectance from each surface approaches zero. Errors in thin film thickness as small as 0.005% can increase the reflectance or reduce the transmittance by 10 percent. The thickness of the layers was therefore monitored during the fabrication process using a collimated halogen light source, blocking filters, UV photomultiplier tube and a 1-meter spectrometer.

4. Absorption must be minimized in order to obtain maximum transmittance in narrow-band interference filters. This is particularly true for layers located near the highest electric field in a thin film stack. Process improvements were made to reduce the absorption coefficient of tantalum pentoxide (Ta_2O_5) from 1.6×10^{-4} to 2.0×10^{-5}. Efforts were also concentrated on optimizing the ion gun and electron gun parameters along with the partial pressure of oxygen during deposition. It was also imperative that the partial pressure of water vapor be minimized.

4 Atmospheric Measurements

Using the processes just described, filters with specifications shown in Table 1 were manufactured at Barr Associates and tested in the NASA/GSFC Mesoscale Atmospheric Processes Raman Lidar

Laboratory. The filters were installed in the Raman Airborne Spectroscopic Lidar (RASL) which was undergoing upward-looking, laboratory-based tests funded through the NASA Instrument Incubator Program. RASL consists of a frequency-tripled Continuum 9050 Nd:YAG laser (17.5W @ 354.7 nm), 0.6 m Dahl-Kirkham telescope operated with 0.25 milliradian field-of-view and wavelength selection using beamsplitters and interference filters. (More system details on RASL are available at http://ramanlidar.gsfc.nasa.gov.)

4.1 Water vapor mixing ratio measurements

Water vapor is one of the most important components of the atmosphere from considerations of both weather and climate yet it is one of the most difficult to quantify due to its high variability on short time and space scales. Advances in water vapor profiling capabilities are sought to improve quantitative precipitation forecasting [Weckwerth et. al., 2004] and to improve our ability to quantify and study mesoscale meteorological systems [Demoz et. al., 2005] [Demoz et. al., 2006] [Wulfmeyer et. al., 2006]. Raman lidar is a well-established technology for profiling water vapor and other quantities in the troposphere. The technology advances in interference filters achieved in this research permits significant improvements in that profiling capability.

On July 26, 2005 RASL was operated from the ground over a period of approximately 14 hours from early morning until late in the evening in order to test its upward-looking measurement capability. The measurements included periods of wbright mid-summer, daytime conditions in the vicinity of Washington, DC where urban haze can significantly increase the sky brightness in the

visible and near-UV, thus degrading daytime measurement performance. The time series of RASL measurements of water vapor mixing ratio, made using filters 1 and 2 listed in Table 1 are shown in figure 1. The data were acquired using 1-minute temporal resolution and 7.5 meter spatial resolution. The data were then processed using a 3-minute sliding window in the time domain and a sliding window in the vertical domain that varied from 90 to 330 meters. The resulting temporal and spatial resolution of the water vapor mixing ratio measurements, determined by the half-power point in a Fourier spectral analysis, was approximately 2 minutes and between 60 and 210 meters, respectively. The measurements were calibrated against the total precipitable water measured by a collocated SuomiNet GPS system [Whiteman et. al., 2006b]. High noon occurred at approximately 1800 UT when the solar zenith angle reached approximately 20 degrees. The daytime boundary layer can be observed in the image at heights that range between 1.5 and 2 km. The residual layer, from boundary layer mixing on previous days, is observed to descend from approximately 4.5 km to less than 3 km over the period of the measurements. Despite the bright conditions present, a moist layer can also be observed descending from 6 km to approximately 5 km during the measurements. Boundary layer convective cells, which supported the development of cumulus clouds at altitudes of 1.5 to 1.8 km, can be observed as vertical striping in the water vapor field between 1800 and 2100 UT. The vertical striping of the image at approximately 16.0 and 19.5 UT are due to clouds that developed at the top of the boundary layer. Times shown with values larger than 24 UT are on July 27 (UT).

A comparison of these RASL measurements made in Greenbelt, MD and a Vaisala RS-80H radiosonde launched from the Howard University Research Campus in Beltsville, MD - a distance of approximately 10 km from GSFC - is shown in figure 2. The location of features in the vertical and the overall calibration of the two measurements are in good agreement. These measurements occurred at 1300 UT when the sun was ~20 degrees above the horizon and daytime mixing in the boundary layer had not yet developed to a significant degree. Therefore, the water vapor field was likely to be reasonably homogeneous between the two sites due to the stable atmospheric conditions of the previous evening. The radiosonde/lidar comparison shown supports the conclusion that the layered features observed in figure 1 are realistic. Furthermore, both figure 2 and comparisons of water vapor mixing ratio measurements derived from the first 30-meters of RASL data and those from a Paroscientific Met3A sensor (not shown) mounted 10 meters above the laboratory in which RASL was located showed good agreement in the lowest portions of the profile even though no overlap correction was applied to RASL data. These facts imply that the lidar system overlap function, which can require height-dependent corrections to compensate for [Whiteman et. al., 2006a], has minimal effect on the RASL mixing ratio measurements presented here. Also, a comparison of the time series of total precipitable water vapor measurements from RASL and GPS showed good agreement except in the presence of clouds, which attenuated the laser beam and prevented full profiling of the atmospheric column.

The random error in the water vapor mixing ratio data was quantified at three times in figure

1 to study the evolution of random errors as a function of sun angle and therefore sky brightness. Figure 3 presents the RASL water vapor mixing ratio profiles and the random error at 13, 18, and 26.5 UT when the solar zenith angles were 70, 20, and -12 degrees respectively. The latter value indicates that the sun was 12 degrees below the horizon. These profiles possess the same temporal and spatial resolution as shown in the image of figure 1. A general characteristic of the upward-looking RASL measurements is the increase in random error below approximately 0.6 km. This is due to reduction of the signal in the near field due to the use of a narrow field-of-view detection scheme. This is one of the consequences of the single field-of-view design of an airborne lidar system intended for downward-looking measurements. A supplemental smaller telescope can be used at wider field of view to reduce the near field random errors [Whiteman et. al., 2006a].

The profiles of mixing ratio shown on the left side of the figure indicate that on this day the boundary layer extended to an altitude of approximately 2 km and was characterized by mixing ratio values ranging roughly from 5-15 g/Kg. A significant residual layer existed between altitudes of approximately 2 and 4 km where mixing ratio values ranged between ~1 and 7 g/Kg. Above the residual layer and up to an altitude of 8 km, mixing ratio values ranged between 1 and 3 g/Kg. The random errors are shown on the right side of the figure indicating that, even at 1800 UT (solar noon), the random error did not exceed 2% in the boundary layer (except for the near-field zone at altitudes less than 0.6 km), 4% in the residual layer and ranged between 20% and 60% above the residual layer up to an altitude of 8 km. The measurements acquired at 1300 UT when the sun was

20 degrees above the horizon possessed less than 3% random error through the residual layer and less than 8% below 6 km. The profile acquired at night possessed less than 7% random error up to an altitude of 8 km.

This measurement quality is to be contrasted with an earlier comparison of the relative error budgets of differential absorption lidar (DIAL) and Raman lidar water vapor measurements. That study [Bösenberg, 2005], based on measurements acquired in Oklahoma in late 1999 by the Max Planck Institute (MPI) water vapor DIAL and the U. S. Department of Energy (DOE) Climate and Radiation Facility Raman Lidar (CARL), indicated that the Raman lidar was not able to provide sufficient temporal and spatial resolution measurements of water vapor in the daytime to permit boundary layer turbulence to be studied. It should be noted that at the time of these comparisons the CARL instrument used a x10 attenuating filter in the water vapor channel during the daytime due to countrate limitations in the data acquisition electronics. The DIAL water vapor measurements acquired during this study possessed 3-7% error between the altitudes of 400 and 1500 meters using 1-minute temporal averaging and 90-meter spatial resolution and were of sufficient quality to permit turbulence studies to be performed. Extrapolations based on the RASL measurements shown in figure 3 indicate that, with the same temporal and spatial resolution and for similar water vapor measurement conditions as for the MPI DIAL/CARL study, the RASL random error would remain below 4% for altitudes less than 2 km and below 7% for altitudes less than 3km, again excluding the near range of ~0.6 km which RASL was not designed to measure with high

precision. The CARL lidar has been upgraded since 1999 so that it no longer uses an attenuation of a factor of 10 in the daytime. CARL daytime water vapor measurements should now be similar to those of RASL shown here. Therefore, CARL can now be expected to provide long-term water vapor measurements that are suitable for boundary layer turbulence studies.

These water vapor random error characteristics are improved over recently-published daytime Raman lidar water vapor measurements acquired during the International H_2O Experiment (IHOP) [Weckwerth et. al., 2004] by the NASA/GSFC Scanning Raman Lidar (SRL) [Whiteman et. al., 2006a] [Whiteman et. al., 2006b]. The analysis of errors from that experiment indicated that, under similar water vapor and sky brightness conditions, the SRL random error did not exceed 10% throughout the boundary layer although the boundary layer rose to greater altitudes. Accounting for the differences in the measurements between the SRL during IHOP and RASL on July 26, 2005, the RASL measurements exhibit approximately a factor of 2 reduction in the random error in the water vapor mixing ratio measurements compared with the SRL during IHOP. This factor of 2 (which requires a factor of 4 more signal, for example, if the background skylight remains constant) can be explained by the combination of a RASL laser that is approximately twice as powerful as the SRL laser and by the newly-developed RASL interference filters that possess approximately twice the peak transmission as the filters in use in the SRL at the time of IHOP.

4.2 Cirrus cloud optical depth and extinction to backscatter ratio

Cirrus clouds strongly influence the radiation balance of the Earth. Some studies have shown that

sub-visual cirrus clouds may cover as much as 70% of the tropics [Wang, 1996] and yet these are the clouds that are most difficult to detect using passive sensors and that can even go undetected during the daytime by low-pulse-energy lidar systems [Comstock et. al, 2005]. Space-based lidar systems such as the current Geosciences Laser Altimetry System (GLAS) [Spinhirne et. al., 2005] and CALIPSO [Liu et. al., 2004], scheduled for launch in 2006, have the ability to detect cirrus clouds globally and develop statistics of cirrus clouds not possible with passive sensors. However, to calculate cirrus cloud optical depths the backscatter measured by space-based lidar must be converted to extinction assuming some value for the extinction-to-backscatter ratio, otherwise known as the lidar ratio. Recent work [Whiteman et. al., 2004] based on earlier cirrus cloud measurements [Whiteman et. al., 2001a] has shown that this value can vary by a factor of two in very cold clouds depending on whether the cloud was hurricane or air-mass-movement induced. Therefore it is important to quantify cirrus cloud properties under a range of measurement conditions to assess the natural range of variability of the cirrus cloud lidar ratio.

Generally Raman lidar measurements of cirrus cloud optical depth and extinction-to-backscatter ratio have not been made in the daytime. The recent use of pure rotational Raman scattering coupled with a Fabry-Perot etalon for temperature profiling has demonstrated the ability to measure cirrus cloud extinction during the daytime [Arshinov et. al., 2005]. But cirrus cloud optical depth measurements during the daytime using the technologically simpler approach of measuring the vibrational q-branch of N_2 have not been demonstrated previously due to poor signal-to-noise

measurements at cirrus altitudes. Using an interference filter produced under this research with a bandwidth of 0.1 nm centered on the Raman vibrational q-branch, Raman lidar measurements of cirrus cloud optical depth and extinction-to-backscatter ratio have been made for the first time using vibrational Raman scattering during the daytime. Figure 4 shows upward-looking RASL measurements of cirrus cloud scattering ratio, optical depth and extinction-to-backscatter ratio calculated with 1-minute temporal resolution. The solar zenith angle was approximately 45 degrees during this measurement period. The statistical uncertainty of both the optical depth and lidar ratio retrievals is less than 10%. The filter passband was centered on the q-branch of N_2 by tilt-tuning of the filter. High resolution spectroscopy indicates that the q-branch of N_2 consists of closely spaced lines over a spectral interval of approximately 5 cm^{-1} [Bendtsen and Rasmussen, 2000]. This translates to approximately 0.075 nm in wavelength space at the Raman shifted wavelength of 386.7 nm. Any variations in laser output wavelength could cause a varying fraction of the q-branch intensity to be transmitted by the filter. Therefore, precise control over the laser wavelength is desirable for an experimental configuration such as this. The Continuum 9050 laser in use in this experiment was not injection-seeded. We observed changes in the transmitted intensity of the Raman N_2 signal when the temperature of the laser cooling water changed by $\pm$5C. We concluded that these transmitted intensity changes were due to variations in the laser output wavelength. Control of the laser cooling water temperature to +/- 1.0C eliminated any noticeable changes in the transmitted intensity of Raman scattering from N_2 as confirmed by Burleigh pulsed wavemeter

measurements. This new cirrus cloud measurement capability will permit Raman lidar systems to provide useful measurements of cirrus cloud optical quantities during both daytime and nighttime.

4.3 Carbon Dioxide

The combination of the use of carbon-based fuels and the reduction in photosynthesis due to the clearing of land has caused concentrations of carbon dioxide (CO_2) and methane (CH_4) to now be higher than they have been for at least 100,000 years. The challenge of accurately modeling and therefore predicting carbon amounts in the atmosphere is illustrated by the high precision required to study some of the key processes driving carbon flux in the atmosphere. Space-based sensors are challenged to measure changes in the column content of CO_2 of less than 1%. However, most of the short-term variation in the column content of CO_2 is occurring within the atmospheric boundary layer where CO_2 concentrations may increase by 5 to 10% overnight particularly closest to the surface [Bakwin et. al., 1998]. Ground-based and airborne sensors are both closer to the region of maximum variation in CO_2 and can be developed more quickly than space-based sensors. Therefore, as space-based systems are developed, it makes sense to pursue attractive ground-based and airborne technologies that can help improve our understanding of the carbon cycle. Using high transmission interference filters fabricated under this research effort, we demonstrate the feasibility of using Raman lidar for the simultaneous profiling of water vapor mixing ratio and carbon dioxide mixing ratio.

4.3.1 Numerical simulations of Raman lidar CO_2 mixing ratio measurements

To study the anticipated signal strength of a Raman lidar measurement of CO_2, a numerical model that was previously validated for measurements of water vapor mixing ratio [Whiteman et. al., 2001b] was used to simulate a ground-based CO_2 Raman lidar system with the RASL specifications of 0.6 meter telescope, 17.5 Watt laser emitting at 354.7 nm, 0.3 nm filters centered on the 2 ν_2 CO_2 Raman transition (1285 cm^{-1}) and the N_2 Raman vibrational q-branch (2330 cm^{-1}). It should be noted that the natural quantity that is measured by a Raman lidar, whether in the case of water vapor [Whiteman et. al., 1992] or CO_2 [Ansmann et. al., 1992b], is the mixing ratio with respect to dry air. This is done by using Raman scattering from molecular nitrogen to normalize the water vapor or CO_2 signal. The numerical model simulates both CO_2 and N_2 signals based on atmospheric input profiles and other quantities [Whiteman et. al., 2001b]. The results are shown in figure 5. The simulations were performed assuming a 5-hour average. The spatial resolution was as follows: <1.25 km: 75m, 1.25 - 2.0 km: 150m, 2.0 - 2.5 km: 250 m, 2.5 - 3.0 km: 400m, above 3.0 km: 600m.

The input to the model included a 10 ppm increase in CO_2 at a height of 2.2 km to simulate the depletion of CO_2 within the mixed layer that occurs during the daytime. Therefore, the input CO_2 profile simulates a possible condition shortly after sunset since these Raman lidar measurements can only be made at night due to the weak nature of the Raman CO_2 signal. As shown in figure 5, the 10 ppm difference between the mixed layer and the free troposphere is easily resolved using

the measurement parameters that were simulated. The precision of the measurement decreases at each change in vertical smoothing such that it remains below 1 PPM at all altitudes up to ~3.5 km using the vertical resolutions mentioned.

On September 19, 2004, RASL was run for 3 hours acquiring what we believe to be the first simultaneous remote profile measurements of atmospheric CO_2 and H_2O mixing ratio. These are likely the first ground-based CO_2 profile measurements extending into the free troposphere as well. The CO_2 measurements were calibrated based on ground-based measurements of CO_2 acquired at the same time. The CO_2 calibration obtained must therefore be considered only approximate. The water vapor measurements were calibrated by forcing the total precipitable water of the lidar profile to equal that measured by a collocated GPS sensor. Both the CO_2 and H_2O have been analyzed such that the vertical resolution is 300 m between 1 and 2 km, 400 m between 2 and 3 km, 500 m between 3 and 4 km, and 600 m above 4 km. The precision of the CO_2 mixing ratio measurement obtained with these resolutions, determined from the signal strength of the CO_2 and N_2 data assuming Poisson statistics, remains below 1.5 PPM for altitudes less than 4 km. The precision of the CO_2 measurement is generally consistent with the model predictions shown in figure 5. The standard error bars plotted on the water vapor mixing ratio data shown in figure 5 are imperceptible on this scale.

Error sources in the measurement of CO_2 using Raman lidar The only known previous

measurements of atmospheric CO_2 ($2\ \nu_2$: 1285 cm^{-1}) using Raman lidar were made by a Ph.D. student [Riebesell, 1990] [?] working at the GKSS Institute in Hamburg, Germany in the late 1980s. The conclusions based on that research were that useful CO_2 measurements by Raman lidar were unlikely because the interference from rotational lines of O_2 was difficult to determine and fluorescence of either optics or atmospheric particles could contaminate the measurement at the ~1ppm level. However, this earlier research was conducted using a XeCl excimer laser, which has an output spectrum that spans approximately 0.4 nm. This broad spectrum makes the separation of O_2 and CO_2 more difficult than the present use of narrow-band interference filters and a Nd:YAG laser with spectral output of ~0.02 nm. Calculations indicate that the contribution of O_2 rotational lines to the measured CO_2 signal in the present configuration is approximately 1% (~3-4PPM). Rotational line strength modeling [Whiteman et. al., 2001b] can be used to account for this contribution reducing the uncertainty in the CO_2 measurement due to O_2 rotational line interference to much less than 1 PPM.

A careful study of fluorescence of both optical components and atmospheric aerosols would be required as a part of further developing and validating a Raman lidar CO_2 profiling system. Preliminary measurements acquired using a scanning spectrometer coupled to a Raman lidar receiver indicated no significant fluorescence contribution in the CO_2 spectral region, even though fluorescence due to aerosols was observed at longer wavelengths during the same measurement period.

5 Summary and Conclusions

Research conducted under the NASA Advanced Component Technology (ACT) Program has resulted in the construction of narrow-band interference filters with approximately twice the transmission of previous technology. This was accomplished while maintaining the same of out-of-band blocking that is required for Raman lidar application. A technique of interference filter construction based on ion assisted deposition (IAD) was found to produce filters with the best overall performance. Considerable effort was expended addressing four separate concerns in filter fabrication: improving spatial uniformity, minimizing scattering losses, minimizing reflection losses and minimizing absorption losses. At the end of the effort, interference filters possessing bandwidths as narrow as 0.1 nm and peak transmissions of twice what was previously possible were produced. However, the yield of spatially uniform filters was somewhat low indicating that more research in process control is required in order to permit easier manufacture of such narrow filters.

Improved Raman lidar measurements were demonstrated using filters produced under this research that were designed to measure Raman scattering from water vapor, nitrogen and carbon dioxide. The measurements were acquired using the Raman Airborne Spectroscopic Lidar (RASL) operating from the ground in an upward-looking configuration. Water vapor measurements possessing 2-minute temporal and 60 - 210 m spatial resolution were presented. Except for a near-range zone of approximately 600 meters, where random errors increase due to the dynamic range

suppression that is inherent in the narrow field-of-view design of RASL, random errors remained below 4% up to an altitude of approximately 4km. This measurement capability is shown to be sufficient to quantify boundary layer turbulence under daytime conditions.

For the first time, cirrus cloud optical depth and extinction-to-backscatter ratio (lidar ratio) were quantified in the daytime using a measurement of Raman vibrational scattering from molecular nitrogen. Using 1-minute temporal resolution, both optical depth and lidar ratio were quantified with approximately 10% uncertainty under daytime conditions where the solar zenith angle was approximately 45-50 degrees. This new measurement capability will permit cirrus cloud statistics to be acquired throughout the diurnal cycle using Raman lidar.

The final measurements that were shown are what we believe to be the first simultaneous remote measurements of atmospheric carbon dioxide and water vapor mixing ratio extending into the free troposphere. The carbon dioxide measurements were approximately calibrated based on a ground-based measurement of CO_2. The random error of the measurements agreed well with predictions based on numerical simulation. Error sources in the measurement of CO_2 using Raman lidar were considered. The interference of rotational lines from O_2 were estimated to be small. Aerosol fluorescence was studied briefly and found to not contribute signal in the spectral band of CO_2. Additional error sources such as the lidar system overlap function and the differential transmission of the atmosphere must also be studied. When all of these error sources are considered, it is unlikely that a Raman lidar measurement of CO_2 with absolute accuracy of 1 PPM could be

achieved. However, for the study of carbon sources and sinks a quantification of nocturnal changes in CO_2 with a precision of 1 PPM (as opposed to an absolute accuracy of a 1 PPM) is sufficient to provide useful information for modeling efforts that are designed to improve our understanding of carbon processes in the atmosphere. Therefore, the results presented here indicate that continued development of Raman lidar profiling of CO_2 is a worthwhile research effort since the signal strength exists for highly precise nocturnal CO_2 profile measurements to be made and for their correlation with H_2O to be studied.

6 Acknowledgements

The authors wish to acknowledge the support of the NASA Advanced Component Technology (ACT) program and Instrument Incubator Program (IIP) for support of these efforts. The radiosonde data were obtained from the Howard University Beltsville Research Campus under a program supported by the Maryland Department of the Environment.

7 References

[Ansmann et. al., 1990] A.Ansmann, M. Riebesell, and C. Weitkamp, 1990: "Measurement of atmospheric aerosol extinction profiles with a Raman lidar," *Optics Letters*, **15**, 13, 746-748.

[Ansmann et. al., 1992a] Ansmann, A., U. Wandinger, M. Riebesell, C. Weitkamp, W. Michaelis, 1992: Independent measurement of extinction and backscatter profiles in cirrus clouds by

using a combined Raman elastic-backscatter lidar, *Appl. Opt.*, 31, No. 33, 7113-7131.

[Ansmann et. al., 1992b] A. Ansmann, M. Riebesell, C. Weitkamp, E. Voss. W. Lahmann, W. Michaelis,1992: "Combined Raman Elastic-backscatter lidar for vertical profiling of moisture, aerosol extinction, backscatter, and lidar ratio, *Appl. Phys. B.*, 55 (1), 18-28.

[Arshinov et. al., 2005] Arshinov, Y. S. Bobrovnikov, I. Serikov, A. Ansmann, U. Wandinger, D. Althausen, I. Mattis, D. Müller, 2005: "Daytime operation of a pure rotational Raman lidar by use of a Fabry-Perot interferometer", *Appl. Opt.*, 44 (17): 3593-3603 (2005).

[Bakwin et. al., 1998] Bakwin, P.S., P. P. Tans, D. F. Hurst, C. Zhao, 1998" "Measurements of carbon dioxide on very tall towers: results of the NOAA/CMDL program", Tellus, 50B, 401-415.

[Behrendt et. al., 2002] Behrendt A, T. Nakamura, M. Onishi, R. Baumgart, T. Tsuda, 2002: "Combined Raman lidar for the measurement of atmospheric temperature, water vapor, particle extinction coefficient, and particle backscatter coefficient", *Appl. Opt.*, 41 (36): 7657-7666.

[Bendtsen and Rasmussen, 2000] Bendtsen, J. and F. Rasmussen, 2000: "High-resolution incoherent Fourier transform Raman spectrum of the fundamental band of $^{14}N_2$", *J. Raman Spectrosc.* 31, 433–438.

[Bösenberg, 2005] Bösenberg, J., "Differential-Absorption Lidar for Water Vapor and Temperature Profiling", in *Lidar Range-resolved Optical Remote Sensing* C. Weitkamp, ed. (Springer Series in Optical Sciences 102, 2005)

[Comstock et. al, 2005] Comstock, J. M., T.P. Ackerman, and G. G. Mace, 2002: "Ground based lidar and radar remote sensing of tropical cirrus clouds at Nauru Island: Cloud statistics and radiative impacts", *J. Geophys. Res.*, 107, 4714.

[Demoz et. al., 2005] Demoz BB, Starr DOC, Evans KD, Lare AR, Whiteman DN, Schwemmer G, Ferrare RA, Goldsmith JEM, Bisson SE, 2005: "The cold front of 15 April 1994 over the central United States. Part I: Observations", *Mon. Wea. Rev.* 133 (6): 1525-1543.

[Demoz et. al., 2006] Demoz, B. C. Flamant, T. Weckwerth, D. Whiteman, K. Evans, F. Fabry, P Di Girolamo, D. Miller, B. Geerts, W. Brown, G. Schwemmer, B. Gentry, W. Feltz, and Z. Wang, 2006: "The Dryline on 22 May 2002 during IHOP-2002: Convective-Scale Measurements at the Profiling Site", *Monthly Weather Review,* Vol. 134, No. 1, 294–310.

[Di Girolamo et. al, 2004] Di Girolamo, P., R. Marchese, D. N. Whiteman, B. B. Demoz, 2004: Rotational Raman Lidar measurements of atmospheric temperature in the UV, *Geophys. Res. Lett.*, 31, L01106, doi:10.1029/2003GL018342.

[Ferrare et. al., 2005] Ferrare, R. A., D.D. Turner, M. Clayton, B. Schmid, J. Redemann, D.

Covert, R. Elleman, J. Ogren, E. Andrews, J.E.M. Goldsmith, and H. Johsson, 2005: Raman lidar measurements of aerosols and water vapor over the Southern Great Plains during the May 2003 Aerosol IOP. *J. Geophys. Res.*, submitted.

[Liu et. al., 2004] Liu, Z., M. Vaughan, D. Winker, C. Hostetler, L. Poole, D. Hlavka, W. Hart, M. McGill, 2004: "Use of probability distribution functions for discriminating between cloud and aerosol in lidar backscatter data", *J. Geophys. Res.*, Vol. 109, D15202, doi:10.1029/2004JD0047

[MacLeod et. al, 1989] H.A. MacLeod, H. A., Thin Film Optical Filters, 2nd edition McGraw-Hill Publishing Co., New York 1989 pp. 412-420.

[Melfi et. al, 1989] Melfi, S. H., D. N. Whiteman, R. A. Ferrare, 1989: "Observation of atmospheric fronts using Raman lidar moisture measurements", *J. App. Meteor.*, **28**, 789-806.

[Pawlewicz, 1998] Pawlewicz, W. T., "Property and processing comparison of optical coatings made by ion assisted evaporation and magnetron sputtering" Proceedings of Materials Research Society Fall Meeting, Boston, 1998.

[Potter and Simons, 1993] Potter, J. R., and J.C. Simons, "Stability of refractory oxide narrowband interference filters" SPIE, vol. 1952, pp. 186-191, April 1993

[Reichardt et. al., 2002] Reichardt, J., S. Reichardt, A. Behrendt, and T. J. McGee, Correlations

among the optical properties of cirrus-cloud particles: Implications for spaceborne remote sensing, Geophys. Res. Lett., 29, 1029-1032, 2002.

[Riebesell, 1990] Riebesell, M., 1990: "Raman-Lidar zur Fernmessung von Wasserdampf- und Kohlendioxid-Höhenprofilen in der Tropsphäre", PhD Thesis, GKSS document 90/E/13, 127 pp.

[Schink et. al., 1995] Schink, H., E. Masetti, M. Montecchi, D. Flori, "Optical absorption of HfO_2 and mixed HfO_2/Al_2O_3 thin films in the 230-700 nm range" Optical Interference Coatings, OSA vol. 17, pp.307-308, June, 1995.

[Spinhirne et. al., 2005] Spinhirne JD, Palm SP, Hart WD, Hlavka DL, Welton EJ, 2005: "Cloud and aerosol measurements from GLAS: Overview and initial results", *Geophys. Res. Lettr.*, 32 (22): Art. No. L22S03.

[Turner et. al., 2000] Turner, D. D., W. F. Feltz, R. A. Ferrare, 2000: "Continuous Water Profiles from Operational Ground-based Active and Passive Remote Sensors", *Bull. Amer. Soc.*, **81**, 1301-1317.

[Wang, 1996] Wang, P.-H., P. Minnis, M. P. McCormick, G. S. Kent, and K. M. Skeens, 1996: "A 6-year climatology of cloud occurrence frequency from Stratospheric Aerosol and Gas Experiment II observations (1985-1990)", *J. Geophys. Res.*, 101, 29,407-29,429.

[Weckwerth et. al., 2004] Weckwerth T. M., D. B. Parsons, S. E. Koch, J. A. Moore, M. A. LeMone, B. B. Demoz, C. Flamant, B. Geerts, J. H.Wang, W. F. Feltz, 2004: "An overview of the International H2O Project (IHOP_2002) and some preliminary highlights", *Bull. Amer. Meteor. Soc.*, 85 (2) 253.

[Whiteman et. al., 1992] Whiteman, D.N., S.H. Melfi, and R.A. Ferrare, 1992: Raman lidar system for the measurement of water vapor and aerosols in the earth's atmosphere", *Appl. Opt.*, **31**, No. 16, 3068-3082.

[Whiteman et. al., 2001a] Whiteman, D.N., K. D. Evans, B. Demoz, D. O'C. Starr, E. Eloranta, D. Tobin, W. Feltz, G. J. Jedlovec, S. I. Gutman, G. K. Schwemmer, M. Cadirola, S. H. Melfi, F. J. Schmidlin, 2001: Raman lidar measurements of water vapor and cirrus clouds during the passage of hurricane Bonnie, *J. of Geophys. Res.*, 106, No. D6, 5211-5225.

[Whiteman et. al., 2001b] Whiteman, D.N., G. Schwemmer, T. Berkoff, H. Plotkin, L. Ramos-Izquierdo, G. Pappalardo, 2001: Performance modeling of an airborne Raman water vapor lidar, *Appl. Opt.*,**40**, No. 3, 375-390.

[Whiteman et. al., 2004] Whiteman, D.N., B. Demoz, Z. Wang: 2004, "Subtropical cirrus cloud extinction to backscatter ratios measured by Raman Lidar during CAMEX-3", *Geophys. Res. Lett.*, 31, L12105, doi:10.1029/2004GL020003.

[Whiteman et. al., 2006a] Whiteman, D.N., B. Demoz, P. Di Girolamo, J. Comer, I. Veselovskii, K. Evans, Z. Wang, M. Cadirola, K. Rush, D. Sabatino, G. Schwemmer, B. Gentry, S. H. Melfi, B. Mielke, D. Venable, T. Van Hove, E. Browell, R. Ferrare, S. Ismail, J. Wang, 2006: Raman Water Vapor Lidar Measurements During the International H_2O Project. I. Instrumentation and Analysis Techniques, *J. Atmos. Oceanic Technol.*, 23, 157-169.

[Whiteman et. al., 2006b] Whiteman, D.N., B. Demoz, P. Di Girolamo, J. Comer, I. Veselovskii, K. Evans, Z. Wang, M. Cadirola, K. Rush, D. Sabatino, G. Schwemmer, B. Gentry, S. H. Melfi, B. Mielke, D. Venable, T. Van Hove, E. Browell, R. Ferrare, S. Ismail, J. Wang, 2006: Raman Water Vapor Lidar Measurements During the International H_2O Project. II. Instrument Comparisons and Case Studies, *J. Atmos. Oceanic Technol.*, 23, 157-169.

[Wulfmeyer et. al., 2006] Wulfmeyer, V. H-S Bauer, M. Grzeschik, A. Behrendt, F. Vandenberghe, E. V. Browell, S. Ismail and R. A. Ferrare, 2006: "Four-Dimensional Variational Assimilation of Water Vapor Differential Absorption Lidar Data: The First Case Study within IHOP_2002", *Mon. Wea. Rev.*, 134 (1), 209–230.

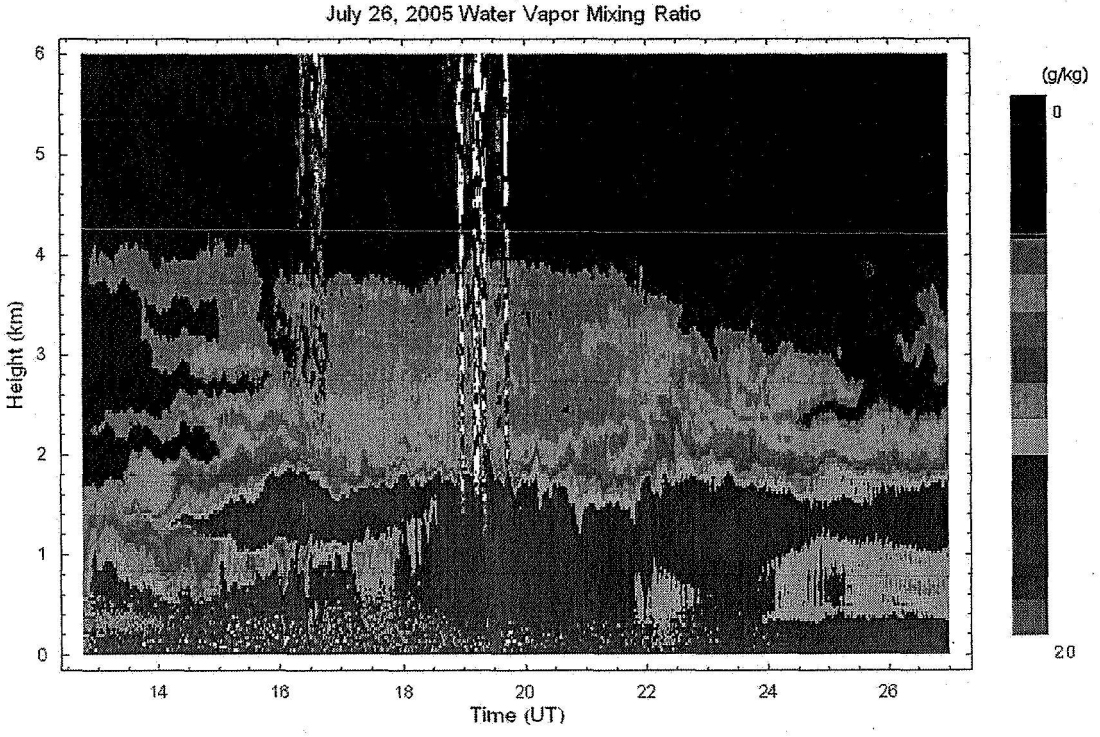

Figure 1: Water vapor mixing ratio measurements made by the upward looking RASL instrument using the narrow band water vapor and nitrogen interference filters developed under this research effort.

8 Figures

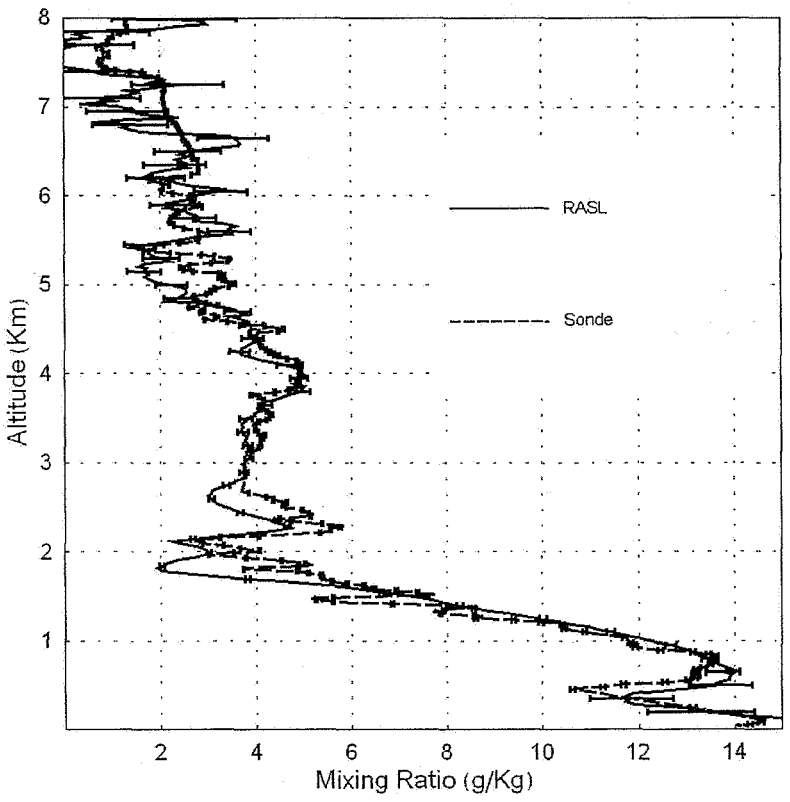

Figure 2: A comparison of RASL measurements of water vapor mixing ratio and those of a radiosonde launched approximately 10 km away. The layering of the features is very similar between these two sites during these early morning measurements.

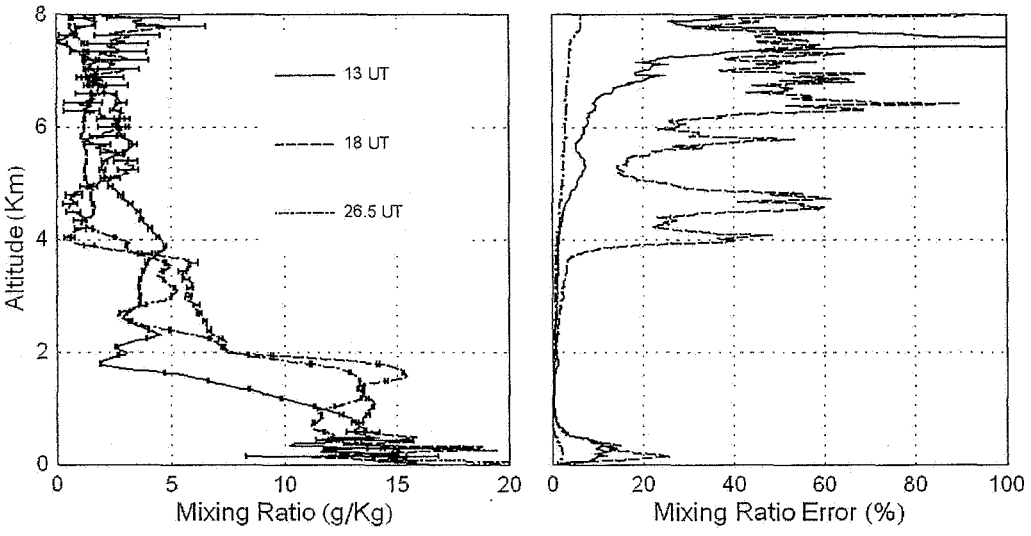

Figure 3: RASL profiles of water vapor mixing ratio and the random error in water vapor mixing ratio measured at 13, 18 and 26.5 UT.

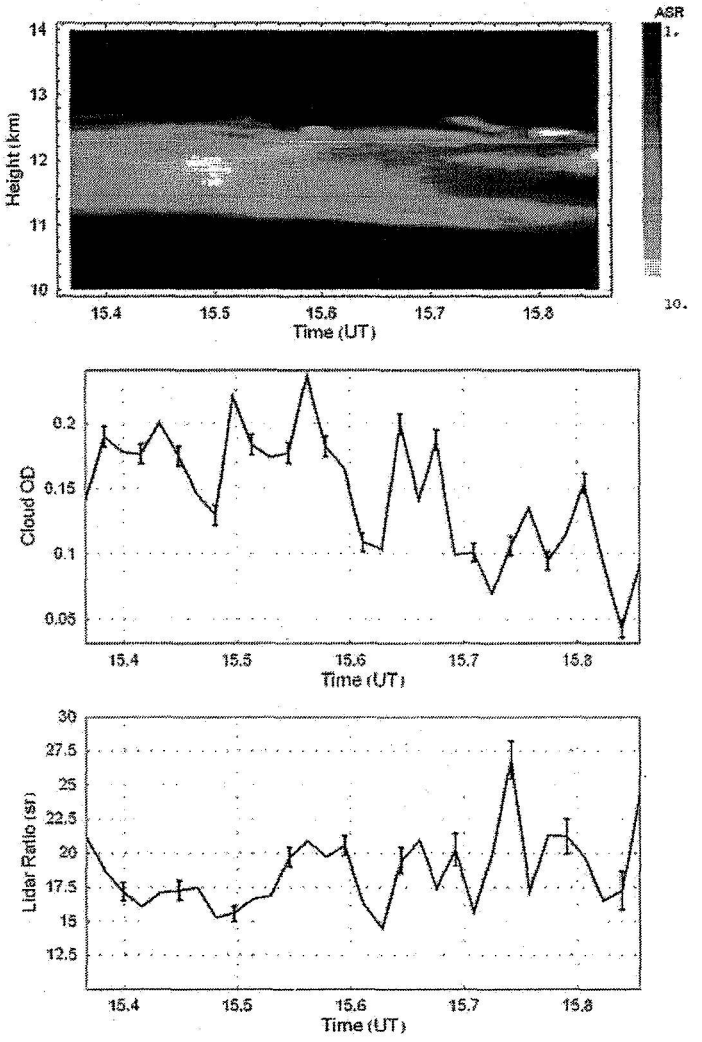

Figure 4: Measurements of cirrus cloud scattering ratio, optical depth and extinction-to-backscatter (lidar) ratio made during the daytime with a solar zenith angle of ~45-50 degrees using 1 minute temporal resolution.

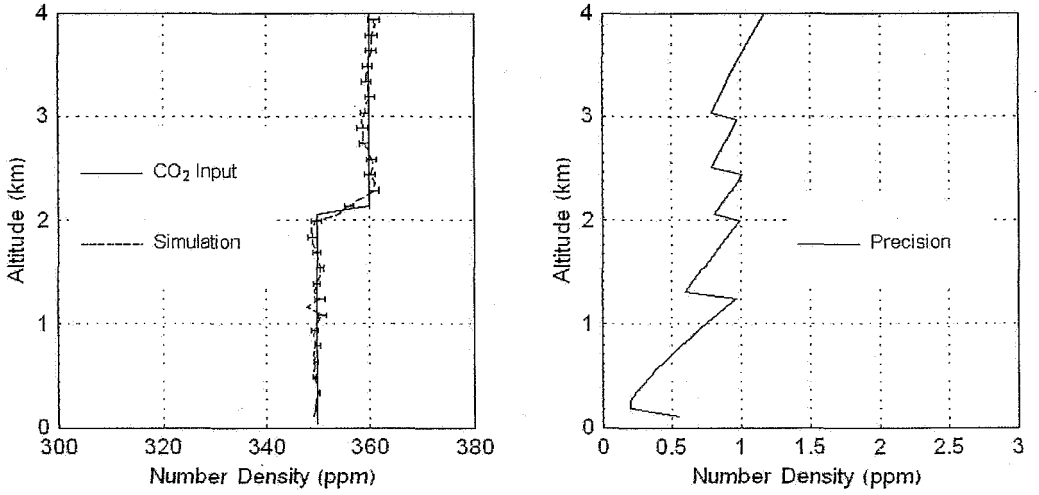

Figure 5: Model simulations of ground-based profiling of CO_2 during the nighttime. The parameters simulated are 0.6 m telescope and 17.5W UV laser with an averaging time of 5 hours. The resultant precision is below 1ppm for all altitudes below 3.5 km with vertical resolution ranging from 75 m to 600 m. A free tropospheric transition was simulated at approximately 2 km where the vertical resolution of the simulation was 250 m.

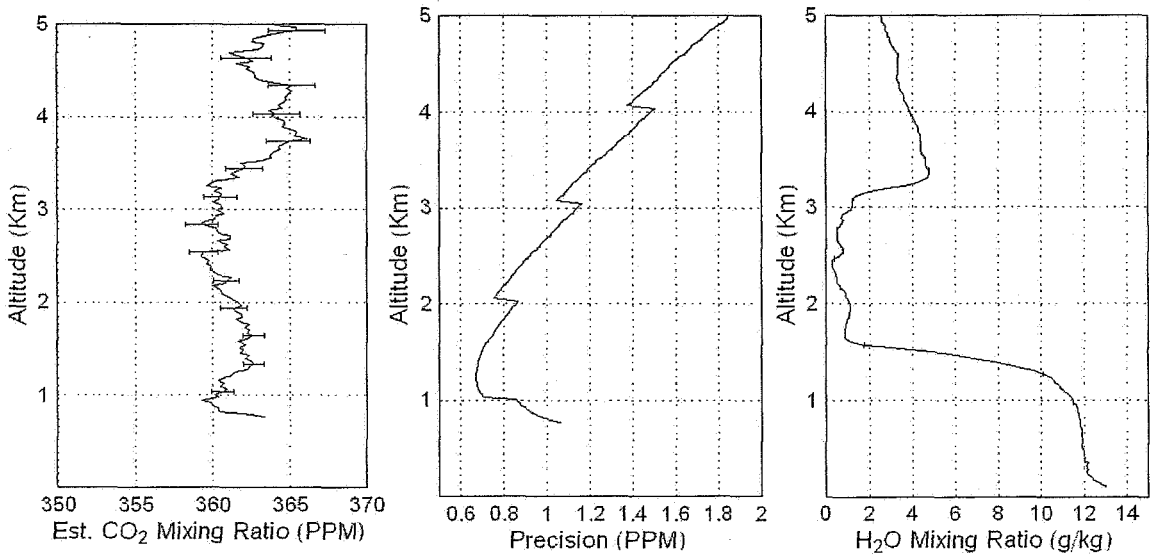

Figure 6: The carbon dioxide mixing ratio is shown on the left using an approximate calibration derived from ground-based measurements. The precision of the CO_2 measurent is shown in the second panel. The simultaneously acquired water vapor mixing ratio measurement is also shown. The averaging time for these measurements was 3 hours.

CWL (+0.02/0.00 nm)	BW (±0.02)	T (%)	General blocking	Additional blocking	Measurement
1) 407.5	0.25	70	OD6 @ 200-1200 nm	OD12 @354.7nm OD8 @ 375-387nm OD9 @532&1064nm	Raman water vapor
2) 386.68	0.1	60	OD6 @ 200-1200 nm	OD12 @354.7nm OD9 @532&1064nm	Raman nitrogen
3) 371.71	0.1	40	OD6 @ 200-1200 nm	OD12 @354.7nm OD7 @375-387nm	Raman carbon dioxide

Table 1: Specifications of interference filters discussed in this article. BW refers to the full width half maximum bandwidth of the filter, CWL to the center wavelength of the filter, T to the transmission.

Material	Surface Roughness (nm RMS)	T (%)
Polished B-270	0.15	43
Polished UV fused silica	0.12	56
Float Soda Lime Glass	0.048	73

Table 2: Substrate surface roughness versus transmission.

9 Tables